THE UNIVERSITY OF MICHIGAN
ANN ARBOR, MICHIGAN

SEMIANNUAL PROGRESS REPORT NO. 7

ON

MICROWAVE DEVICE INVESTIGATIONS

This report covers the period October 1, 1969 to April 1, 1970

Electron Physics Laboratory
Department of Electrical Engineering

By: W. R. Curtice
W. D. Getty
G. I. Haddad
R. J. Lomax

Approved by:

G. I. Haddad, Director
Electron Physics Laboratory

Project 08400

RESEARCH GRANT NO. NGL 23-005-183
OFFICE OF SPACE SCIENCE AND APPLICATIONS
NATIONAL AERONAUTICS AND SPACE ADMINISTRATION
WASHINGTON, D. C. 20546

April, 1970

TABLE OF CONTENTS

LIST OF ILLUSTRATIONS

PAPER PRESENTED DURING THE LAST PERIOD

W. D. Getty and V. P. Bhatnagar, "Beam-Plasma Interaction Near the Lower Hybrid Frequency," Presented at the Eleventh Annual Meeting of the Division of Plasma Physics of the American Physical Society, Los Angeles, Calif., November 1969.

SEMIANNUAL PROGRESS REPORT NO. 7

ON

MICROWAVE DEVICE INVESTIGATIONS

1. General Introduction (G. I. Haddad)

The purpose of this program is to investigate materials, devices and novel schemes for generation, amplification and detection of millimeter-wave energy. Several tasks are presently active under this program and the status of each one is described in the following sections of this report. Considerable progress has been made in the various tasks and several publications are presently being prepared. The tasks which were active during this report period are:

1. The study of cyclotron harmonic instabilities.
2. Millimeter- and submillimeter-wave detectors.
3. Millimeter-wave Gunn-effect devices.
4. Avalanche-diode oscillator analysis.

2. Beam-Plasma Interactions

Supervisor: R. J. Lomax

Staff: J. D. Gillanders

2.1 Introduction. The presence of gain or of an instability in a beam-plasma interaction can be determined by examining the dispersion equation of the interaction. Simplified theories which ignore collisions, finite temperature effects and some or all of the boundary conditions predict gain and instabilities much stronger than are observed experimentally. In the simplest cases infinite gains are predicted. However, when the above factors are not ignored, the dispersion relation becomes more complicated. Therefore, a very efficient method is needed to solve the equation if information about the interactions is to be obtained in a reasonable amount of computation time. A new approach to this problem has been outlined in previous reports.

2.2 Conclusions. A draft of a technical report covering this work has been prepared which describes the methods used and results obtained in this investigation. In reviewing the draft it was decided that for a modest additional effort the utility of the method could be much improved by making the computer program more automatic in certain cases and by documenting the application to further wave-interaction systems of interest. In addition the instability analysis program can be made much easier to use if a computer display output is used interactively. This improvement is being implemented.

2.3 Program for the Next Period. The necessary work to incorporate the improvements should be completed and the results included in the final form of the technical report. As soon as this is accomplished this phase of the program will be terminated.

3. The Study of Cyclotron Harmonic Instabilities

Supervisor: W. D. Getty

Staff: A. Singh

3.1 Introduction. This study is concerned with the properties of waves on a neutralized electron beam immersed in a homogeneous axial magnetic field. The electrons in the beam are assumed to have an appreciable amount of velocity in a plane perpendicular to the magnetic field.

An electron beam of this type can be considered as a plasma with an anisotropic electron velocity distribution function. Theoretical wave studies have shown that such a plasma cen support propagating waves in narrow passbands near the electron-cyclotron frequency and its harmonics. Under certain conditions these waves become unstable and it is possible for the system to behave as a self-excited oscillator near one or more of the cyclotron harmonics. Application of this phenomenon could be made in the areas of millimeter-wave power generation and ionospheric wave propagation studies from satellites.

The cyclotron harmonic waves are, essentially, electrostatic waves that propagate at nearly right angles to the magnetic field. They are closely related to the electromagnetic waves involved in the cyclotron-resonance-maser-type of millimeter-wave oscillator studied by Kulke.[1]

In this project a detailed study is being made of an electron beam with axial and perpendicular velocity. The electron beam is generated in a triode electron gun and flows along an axial magnetic field through a drift region. Before entering the drift region the beam passes through a spatially helical dc magnetic field that converts part of the axial beam energy into perpendicular energy. Thus each electron follows a helical path through the drift region and the desired velocity distribution is created. The resulting electron gyroradii are comparable to the beam radius.

In the first series of experiments, an axial velocity analyzer was used to measure the velocity distribution characteristics of the electrons after they passed through the helical magnetic field generated by a corkscrew-type coil.[2] The data show satisfactorily that the expected amount of conversion takes place and also that the beam current-density distribution

---

1. Kulke, B., "Millimeter-Wave Generation with Electron Beam Devices," Report No. NASA TN-D-3727, National Aeronautics and Space Administration, Electronics Research Center, Cambridge, Mass., February 1967.

2. Wingerson, R. C., Dupree, T. H. and Rose, D. J., "Trapping and Loss of Charged Particles in a Perturbed Magnetic Field," Phys. Fluids, vol. 9, No. 7, pp. 1475-1484, September 1964.

becomes very nonuniform at the output of the corkscrew. These results are in reasonable agreement with theoretical predictions obtained by computer solution of the trajectory equations. The details of this comparison are presented in this report.

The second series of experiments are concerned with studies of wave propagation along the anisotropic electron beam. Preliminary results have been obtained and are in the process of being evaluated.

3.2 Velocity Conversion Characteristics of the Corkscrew. Experimental and theoretical work on the axial-to-perpendicular velocity conversion characteristics of the corkscrew have been completed. Some typical experimental results and analog computer studies of the device were reported in our previous reports. The analog computer studies showed more severe velocity spreads than those experimentally observed. Digital computer studies made during this period have shown that the discrepancies in the experimental and calculated results were due to the simplifying assumptions made in the analysis.[2] The motion of electrons launched at various phase angles and radii has been studied and some of the important results obtained are reported here.

Figure 3.1 shows $v_{\perp}/v_o$ at the output of the corkscrew as a function of their initial phase angle X_o for particles launched at four different radii (r_o). The angle X_o is the angular position of the particle measured with respect to the direction of the maximum of the radial magnetic field. The particles are assumed to be launched with an initial axial velocity v_o and zero perpendicular velocity. Space-charge effects have been ignored in making these calculations. Figure 3.1 clearly shows that the windup ratio $v_{\perp}/v_o$ is independent of the initial phase angle but is a strong function of initial radius r_o. The radial dependence of $v_{\perp}/v_o$ is clearly shown in Fig. 3.2 where $v_{\perp}/v_o$ is plotted against r_o.

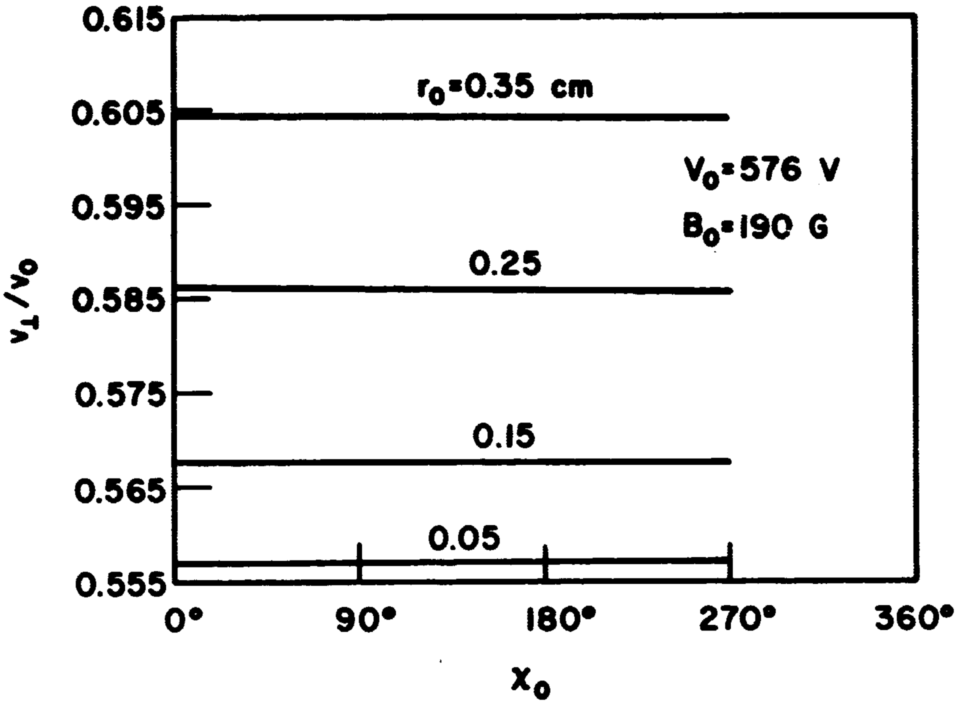

FIG. 3.1 $v_\perp/v_o$ VS. X_o, THE INITIAL PHASE ANGLE OF THE ELECTRONS WITH RESPECT TO THE MAXIMA OF THE TRANSVERSE MAGNETIC FIELD.

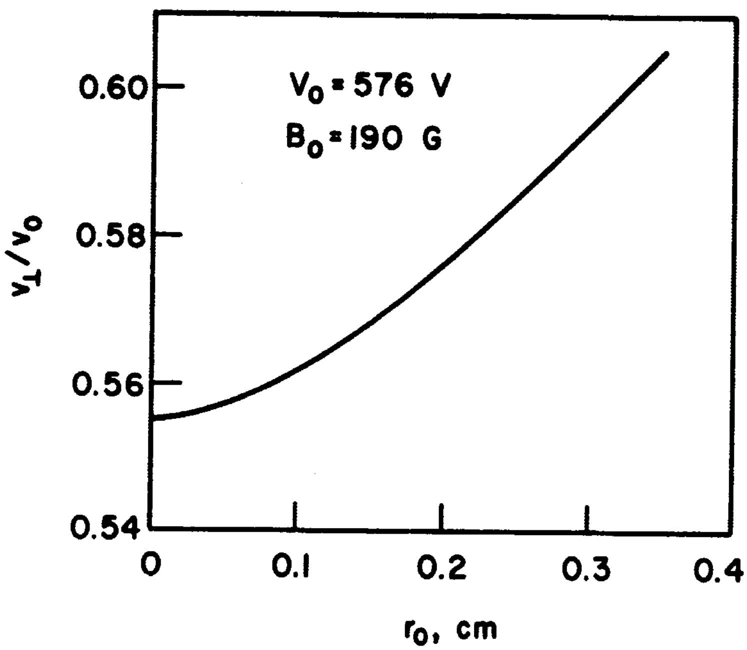

FIG. 3.2 $v_{\perp}/v_o$ VS. INITIAL RADIUS r_o OF THE PARTICLE. ($\chi_o = 0$)

Figure 3.3 shows how a homogeneous electron beam in passing through the corkscrew develops an inhomogeneous density profile. The concentric circles are rings of charge at the input to the corkscrew. The eccentric dashed circles represent the positions that these rings take at the output of the corkscrew. The beam is compressed on the left-hand side and rarefied on the right-hand side of the diagram. This behavior, i.e., relative phase slippage between various rings of charge, can be explained on physical grounds.[2] Figure 3.3 also shows that the point of entry of a particle acts as a fixed guiding center during its journey through the corkscrew.

Other important conclusions that emerge from our numerical studies are the following:

1. If the electrons are launched with some initial perpendicular energy, the velocity-conversion characteristics are very sensitive to the initial angular positions of the particles. The results are very similar to those obtained on an analog computer and given in the last report.

2. A corkscrew designed for a given conversion ratio, beam voltage V_o and axial magnetic field B_o, will give the same velocity conversion characteristics for other beam voltages and axial magnetic field strengths provided the ratio $\sqrt{V_o}/B_o$ is held at the design value and corkscrew current is suitably scaled.

3.3 <u>Axial Magnetic Field Tuning for Minimization of Velocity Spread</u>. In previous reports it had been observed that the spread in the axial velocity of the electrons at the output of the corkscrew can be minimized by operating the device at an axial magnetic field strength that is a little less than the design value. This observation was confirmed by analog computer results. However, Kulke[3] has observed in his experiments that the axial

3. Kulke, B., Private Communication.

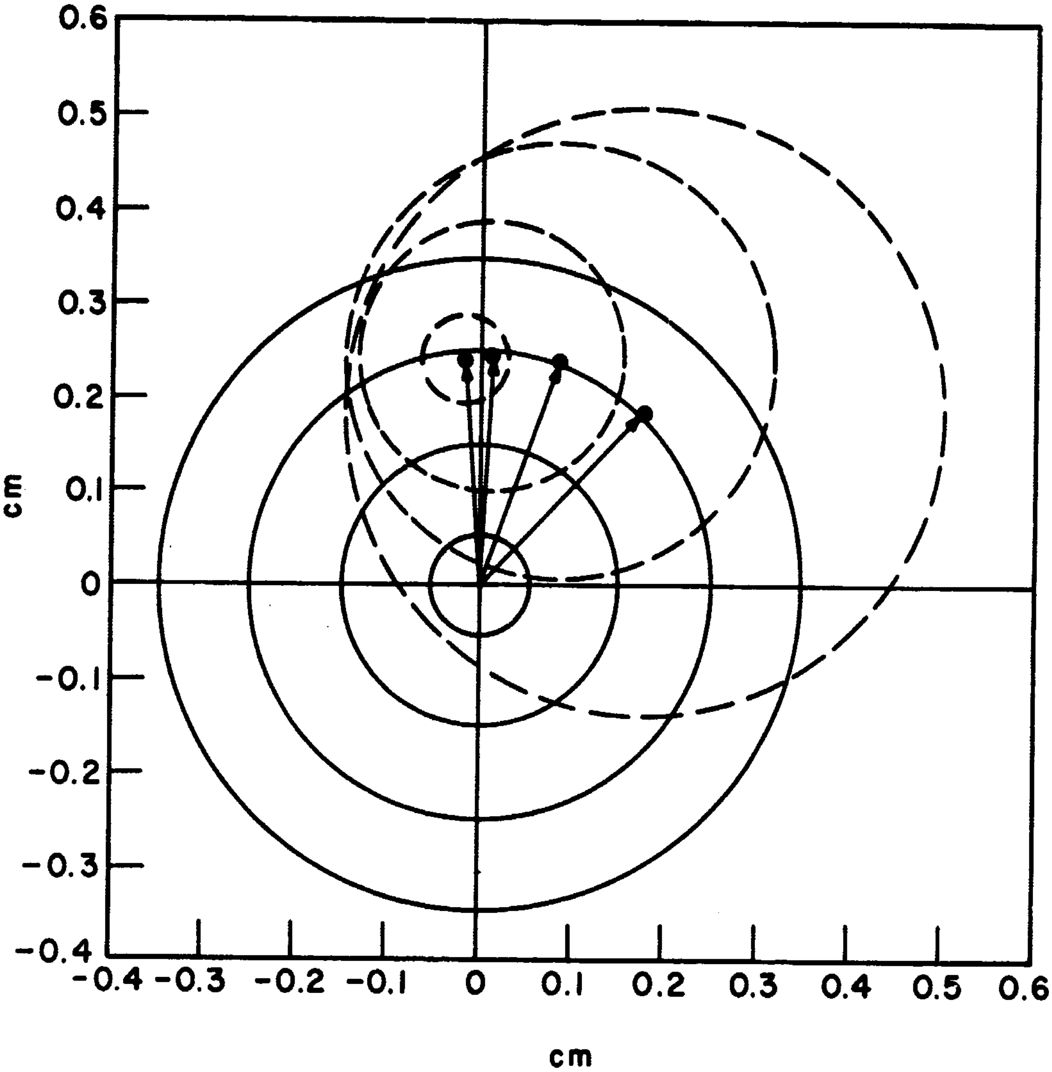

FIG. 3.3 BEAM PROFILE AT THE INPUT AND OUTPUT OF THE CORKSCREW. THE INPUT RADII ARE 0.05, 0.15, 0.25 AND 0.35 cm. THE ARROWS INDICATE THE DISPLACEMENT OF THE CENTERS OF THE FOUR CIRCLES. (V_o = 576 V, B_o = 190 G)

magnetic field has to be increased from the design value for compression of the axial velocity spread. Kulke's observation can be explained with the help of Fig. 3.4, where the computed ratio v_z/v_o at the output of the corkscrew is plotted against the axial magnetic field strength B_o. Other beam parameters are held constant at their design values. The design value of B_o here is 190 G. It can be seen from this figure that as B_o is increased, the difference in axial velocities decreases. The converse is true when B_o is decreased below 190 G. Thus the computer results agree with Kulke's experiment. These curves also explain another observation that the maximum velocity conversion ratio and minimum velocity spread cannot be realized simultaneously. The maxima of $v_\perp/v_o$ correspond to the minima of v_z/v_o. As is seen from Fig. 3.4 the minimum of v_z/v_o occurs at axial magnetic field strengths a little below the design value whereas the minimum spread occurs a little above the design value.

The electron beam used by Kulke meets the ideal conditions used in the above computations. His beam current is of the order of 100 μA at a beam voltage of about 3 kV so that space-charge effects are negligible. This fact, coupled with the comparatively high axial magnetic field (~ 450 G) gives a fairly straight and parallel electron beam with minimal transverse velocity at the input to the corkscrew.

In the experiment carried out here, the electron plasma density of the beam has to be made large compared to the electron-cyclotron frequency in order to realize cyclotron instabilities. Higher space-charge densities coupled with lower values of the axial magnetic fields give rise to a rotational motion to the beam before it enters the corkscrew. This in turn leads to lower $v_\perp/v_o$ ratios and different axial magnetic field tuning characteristics for compression of velocity spread as noted earlier.

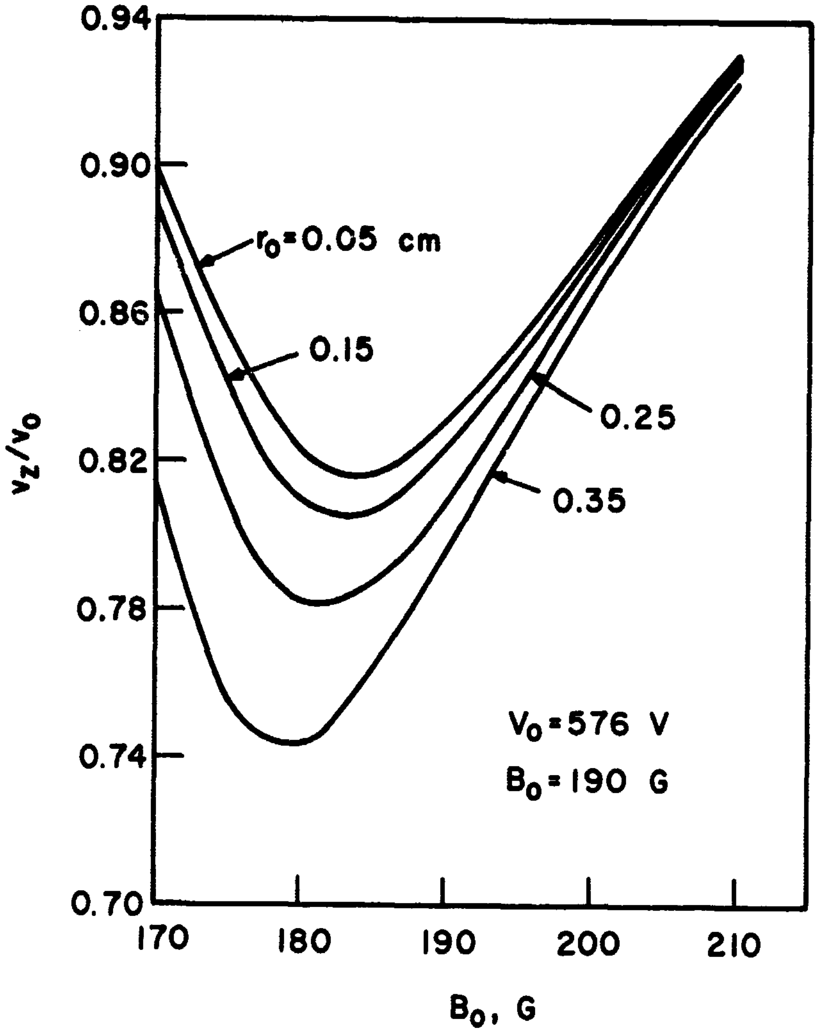

FIG. 3.4 v_z/v_o VS. AXIAL MAGNETIC FIELD B_o WITH INITIAL RADIUS AS A PARAMETER.

Figures 3.5 and 3.6 show comparisons between the computed and the experimentally observed results. In Fig. 3.5 $v_{\perp}/v_o$ is plotted against the axial magnetic field strength. Curves 1 and 2 are computed results for two electrons launched at initial radii of 0.35 cm and 0.05 cm, respectively. Curve 3 is drawn from the experimental data. Curve 4 is drawn by shifting Curve 3 upwards on the B_o/B_{oo} axis by about 7.7 percent. As can be seen the observed and computed results show reasonable agreement in view of the nonideal beam conditions discussed above.

Figure 3.6 shows the variation of $v_{\perp}/v_o$ as a function of the initial voltage. The computed and observed results here agree only over a narrow range of beam voltages. In addition, the experimental data show oscillatory behavior with respect to the beam voltage. A similar effect has been observed by others.[4] At this stage the reasons behind these differences in the results are not understood.

3.4 Study of Cyclotron Harmonic Waves. The device being used for the study of cyclotron harmonic waves was briefly described in the last report. Microwave apparatus for the measurement of dispersion characteristics of the cyclotron harmonic waves is being streamlined to obtain consistency in results and to remove extraneous effects. A block diagram of the microwave measurement setup is shown in Fig. 3.7. The microwave signals picked up from the beam are 20 to 30 dB below the evanescent modes excited by the input coupler in the device. To differentiate these weak signals the electron beam is density modulated at 1 kHz by pulsing the control grid of the electron gun. The signal picked up by the movable RF

4. Dreicer, H., Karr, H. J., Knapp, E. A., Phillips, J. A., Stovall, E. J., Jr. and Tuck, J. L., "Cyclotron Resonance in the Static Magnetic Field of a Helix," Nuclear Fusion Suppl., Part 1, pp. 299-312, 1962.

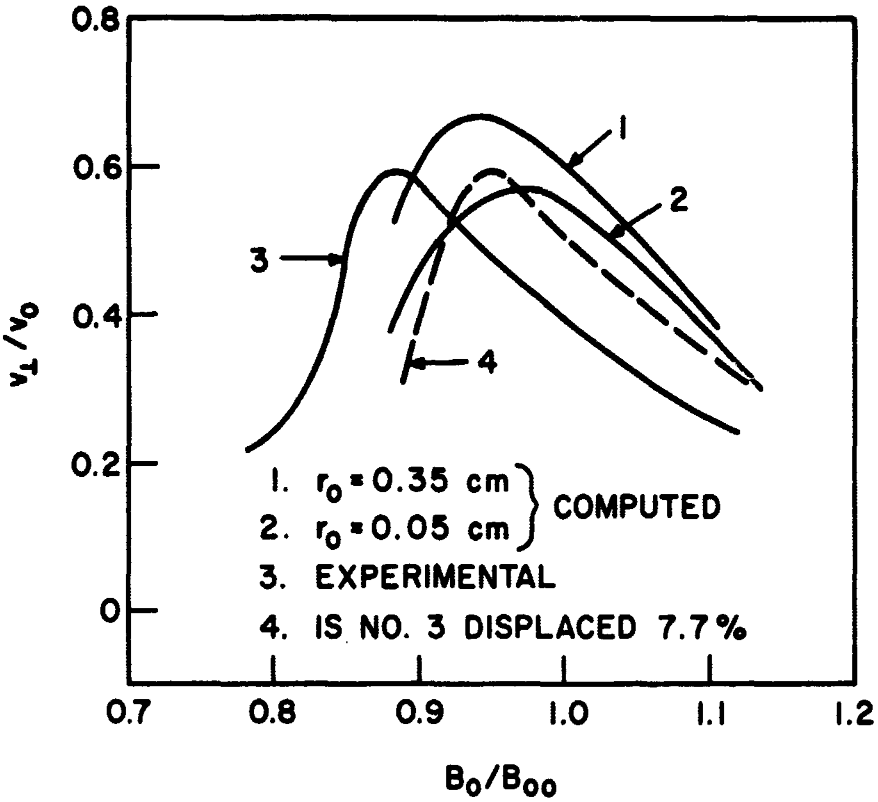

FIG. 3.5 $v_\perp/v_o$ VS. AXIAL MAGNETIC FIELD (B_o)/DESIGN VALUE OF AXIAL MAGNETIC FIELD (B_{oo}). (V_o = 200 V, B_{oo} = 111 G, X_o = 0)

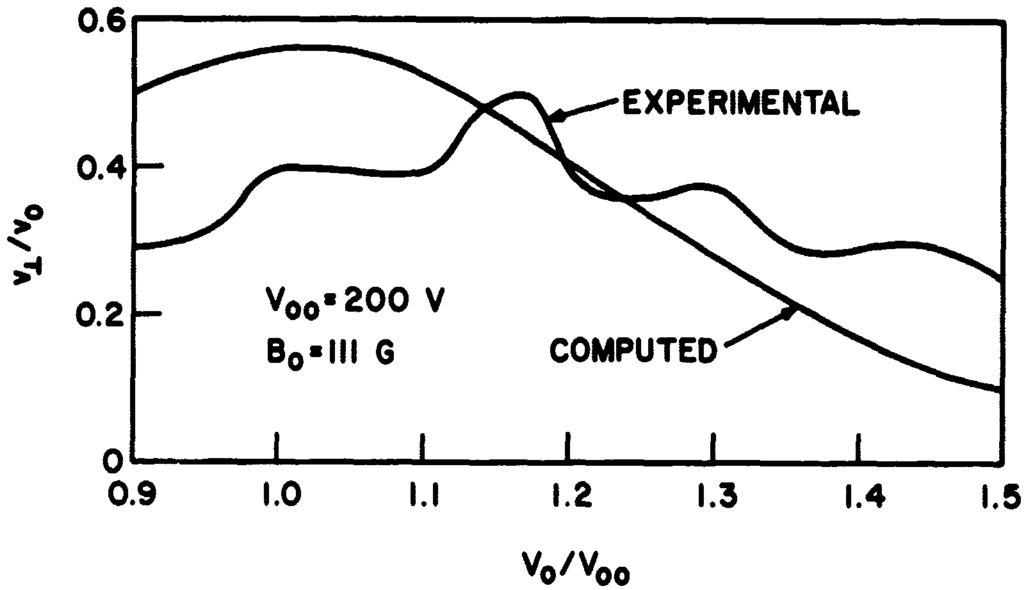

FIG. 3.6 $v_\perp/v_o$ VS. BEAM VOLTAGE (V_o)/DESIGN VALUE OF THE BEAM VOLTAGE (V_{oo}).

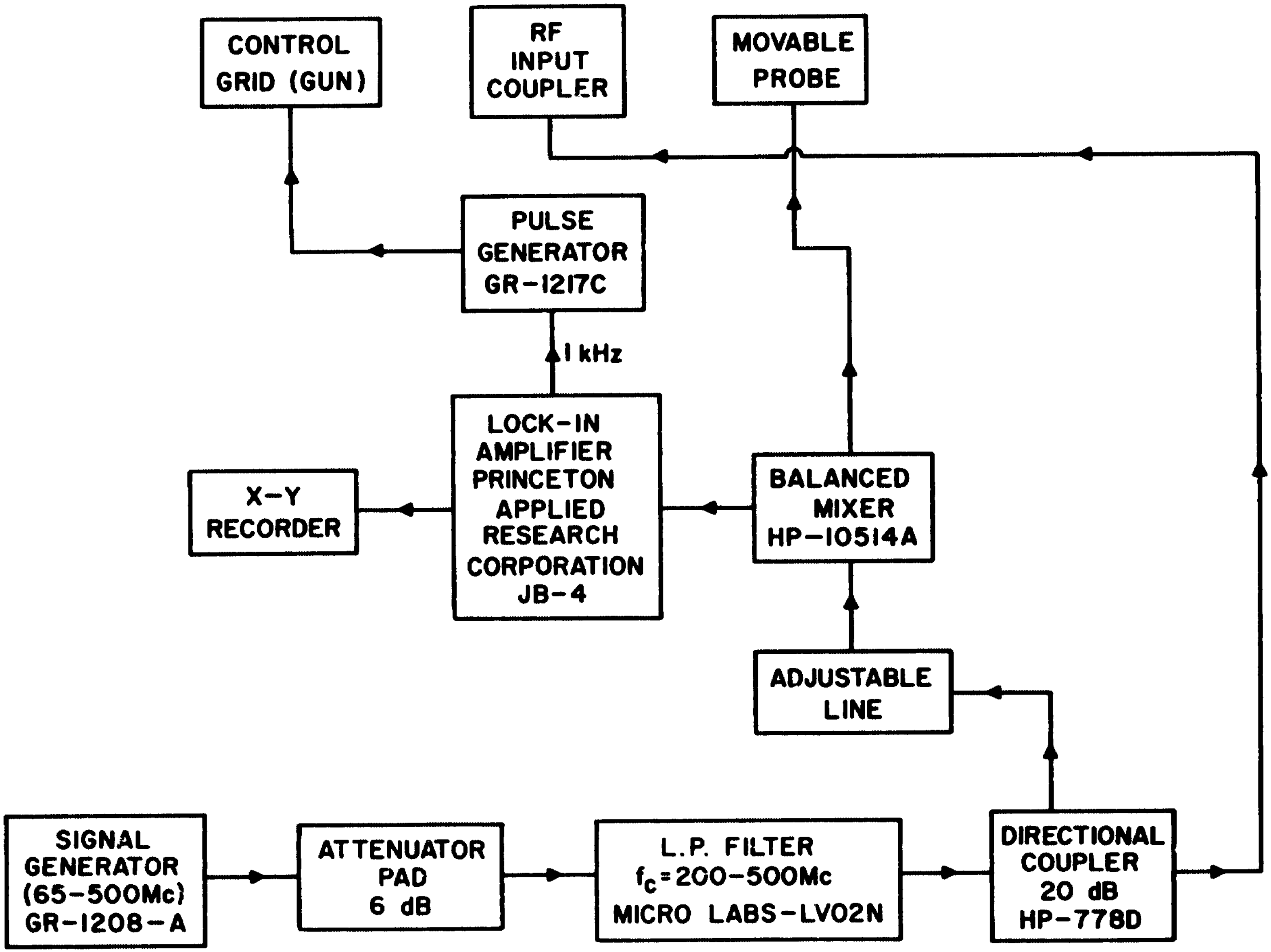

FIG. 3.7 MICROWAVE SETUP FOR THE STUDY OF CYCLOTRON HARMONIC WAVES.

probe is mixed with a reference signal of the same frequency in a balanced mixer. The output of the balanced mixer is fed to a lock-in amplifier which rejects the other components from the output of the balanced mixer and amplifies and rectifies the desired 1 kHz signal. The output of the lock-in amplifier is fed to one axis of an x-y recorder. The other axis is fed from a potentiometer coupled to the motorized drive that is used for probe movement in the vacuum system.

Some initial runs have been made. The data obtained shows basic qualitative features of the expected cyclotron harmonic waves. More than one wave is launched on the beam at a given frequency. Some numerical or experimental techniques will be necessary to extract the values of propagation constants from the experimental data.

3.5 Program for the Next Period. The measurement setup will be refined further to obtain data free from unwanted disturbances. Necessary experimental or numerical techniques will be developed for proper evaluation of the experimental results.

4. Millimeter- and Submillimeter-Wave Detection by Paramagnetic Materials

Supervisor: G. I. Haddad

Staff: C. F. Krumm

4.1 Introduction. This phase of the program was concerned with a study of millimeter- and submillimeter-wave detection by paramagnetic materials. A detailed technical report on this phase of the program has been completed and will be available shortly. The abstract from this technical report is included below.

4.2 Abstract of Forthcoming Technical Report. The purpose of this study is to investigate the use of certain paramagnetic materials for downconversion of millimeter- and submillimeter-wave radiation to microwave frequencies. The conversion scheme utilizes three energy levels associated with the ground state of a paramagnetic material. One pair of these levels is separated by a microwave frequency and another pair by a millimeter-wave frequency. Power applied at the millimeter-wave frequency causes the spin population to redistribute itself among the levels and causes a corresponding change in the power absorbed at the microwave frequency. The overall effect is that changes in the millimeter-wave power level cause corresponding changes in the microwave power absorption.

The downconversion process is analyzed using a microscopic approach. The results of this analysis indicate that the downconversion loss is minimized when the microwave input power approaches the saturation level. Under these conditions the microscopic conversion loss approaches the fundamental limit which is shown to be the ratio of the microwave frequency to the millimeter-wave frequency. The response time of the downconverter is also shown to improve with increasing microwave power input. Both of these predictions have been verified experimentally.

The microscopic results are used to develop an equivalent circuit for the downconverter. This circuit is used to analyze the downconverter performance. The dependence of the conversion loss on mismatch, frequency and magnetic field tuning and saturation is determined. The minimum detectable millimeter-wave input power when a given type of microwave receiver is employed is also evaluated. It is shown theoretically and has been verified experimentally that the minimum detectable power exhibits a minimum as a function of the microwave input power level.

An experimental program was undertaken to demonstrate the feasibility of using downconversion as an alternative to direct detection at millimeter- and submillimeter-wave frequencies. Using iron-doped rutile as the conversion medium, downconversion has been achieved at both liquid nitrogen and liquid helium temperatures. The experimental performance of this device is in substantial agreement with the theoretical predictions. Terminal to terminal conversion losses as low as 15 dB were observed at liquid helium temperatures. The observed response times were on the order of milliseconds at 4.2°K and tens of microseconds at 77°K. The noise equivalent power observed in these initial experiments indicates that the sensitivity of this device is comparable to that of a video detector. The major portion of the work was carried out at 35 GHz where equipment was available. The microwave signal was chosen at 9 GHz. The measured noise equivalent power on the present system was approximately -70 dBm. This can be reduced to approximately -90 dBm by an improved design of the system.

4.3 Program for the Next Period. This work has been completed and no further work is planned for this phase of the program at the present time.

5. Bulk Semiconductor Materials for Millimeter- and Submillimeter-Wave Detection

Supervisor: G. I. Haddad

Staff: I. I. Eldumiati

5.1 Introduction. This part of the program is concerned with the study of bulk semiconductor materials suitable for applications in the millimeter- and submillimeter-wave region. The feasibility of using these materials for radiation detection in this frequency range is to be investigated. Cavity perturbation techniques using field theory and equivalent circuit analyses are being used for this purpose. The principle of operation of the detection scheme was outlined in Semiannual Progress Report No. 3. In this scheme the semiconductor material is placed in a cavity which is simultaneously resonant at the millimeter-wave frequency to be detected and at some X-band frequency. The millimeter-wave signal will cause a change in the material properties, which in turn will cause a change in the reflected X-band signal. The millimeter-wave signal is then detected by monitoring the change in the reflected X-band signal. The cavity perturbation approach was outlined briefly in Semiannual Progress Report Nos. 5 and 6.

5.2 Theoretical Study. Materials suitable for applications in the millimeter- and submillimeter-wave region should have a small energy gap and a small effective mass. This will cause the conduction and impurity bands to merge together even at low temperatures which suggests the use of a two-band conduction model to investigate the properties of these materials. This model was used to derive the dependence of the conductivity and the dielectric constant of the material on the incident radiation in the presence of a magnetic field. In the analysis a hydrogenic model was utilized, the impurity ions were assumed to be arranged on a uniform lattice and the carriers were assumed to have a Maxwellian distribution. An expression for the magnetic field required to freeze out the carriers in the impurity band has been derived.

A computer program to express the relative change in the material's conductivity and dielectric constant was developed. This program allows fitting of the theoretical and experimental results which makes it possible to deduce the mobility and the dielectric relaxation time of the material as a function of the temperature.

5.3 Experimental Investigation. A new experimental cavity system was designed and constructed. In this setup a sample of InSb is placed in the high-field region of a reentrant-type cavity which is coupled to an

X-band and a millimeter-wave signal simultaneously. The cavity system was sealed in vacuum in order to overcome the problems arising from liquid nitrogen cooling and eliminate the effect of humidity on the resonance frequency shift and the change in the coupling factor measurements. This cavity system will also allow testing of the feasibility of the detection scheme outlined earlier. Extensive and detailed experimental tests to determine the material properties as a function of the magnetic field at X-band were carried out at 77, 150, 200 and 300°K. The experimental results were numerically fitted to the theoretical ones and the mobility and dielectric relaxation time were determined at these temperatures. The same tests were carried out at liquid helium temperature.

The detection scheme was tried at liquid helium temperature and it worked satisfactorily both at Ka- and E-bands. Experiments were carried out at 35 and 82 GHz. The response time of the detector was measured by using a square-wave signal to switch the millimeter-wave klystron on and off, and observing the detected signal. The results show that the response time of the detector is better than 4 μs which corresponds to the maximum rate at which the klystron could be modulated. Preliminary measurements indicate a tangential sensitivity of about -40 dBm with the present system. This tangential sensitivity can be lowered considerably by improving the design of the current system. Better tangential sensitivity can be obtained by optimizing the coupling at the millimeter-wave frequency and adding a low-noise microwave amplifier, such as a tunnel diode one, in series with the reflected X-band signal.

5.4 Program for the Next Period. Further detailed theoretical and experimental investigations of the detection scheme will be continued. This will include a more accurate measurement of the time constant and means for improving the tangential sensitivity of the system. Also the feasibility of the detection scheme at liquid nitrogen temperature will be investigated.

6. Millimeter-Wave Gunn-Effect Devices

Supervisor: W. R. Curtice

Staff: J. J. Purcell

6.1 Introduction. The theoretical studies have been completed and a journal article is being prepared. The abstract of this article appears below.

6.2 Abstract of Forthcoming Journal Article. A theoretical analysis is presented of the effects of intervalley transfer time, travel of an accumulation layer and dipole domain growth upon LSA mode operation of GaAs devices. A modified two-valley model is used with energy relaxation effects included to analyze a crystal divided into an active section (above threshold electric field) and a passive section (below threshold field) by an accumulation layer. Domain growth occurs in the active section. Specific results are given for crystal lengths of 20 μm and 100 μm and the influence of crystal parameters and operating conditions upon the conversion efficiency and device RF admittance is discussed.

6.3 Program for the Next Period. Experiments with epitaxial gallium arsenide devices in the Ka-band circuit described previously will be continued.

7. Analysis of Avalanche-Diode Oscillators

Supervisor: R. J. Lomax

Staff: M. S. Gupta

7.1 Introduction. A self-consistent one-dimensional large-signal analysis of a Read-type avalanche diode has been developed which takes into account the device-circuit interaction. The circuit is modeled by a lumped-equivalent network representing the diode package and a coaxial-line cavity with tuning slugs. The circuit parameters for this model were obtained from measurements of actual avalanche-diode circuits. The circuit admittance was calculated over a wide frequency range (from less than 80 MHz to more than 20 GHz) on the assumption that high-order modes were absent in the coaxial-line circuit. It was not necessary to assume the voltage waveform across the diode beforehand; instead the voltage and current waveforms are determined in an iterative manner by satisfying alternately the equations for the diode model and for the circuit.

7.2 Conclusions. A computer program has been written which carries out the analysis described above. In agreement with experimental results it was found that the waveform of the voltage across the diode is strongly dependent upon the circuit connected across the diode. The results indicate that by adjustment of the operating conditions it is possible to get voltage waveforms which are essentially single frequency, with very little harmonic content, or wavefunctions with several prominent harmonics present. These results can be explained in terms of admittance plane plots.

7.3 Program for the Next Period. This phase of the program has been completed and a publication summarizing the results is presently being prepared. No further work is planned on this phase of the program.

8. Noise Modulation in Avalanche-Diode Devices

Supervisor: R. J. Lomax

Staff: M. S. Gupta

8.1 Introduction. A study of the noise in avalanche-diode devices was initiated in this period. While noise studies are an essential part of all microwave device investigations, for avalanche diodes they become even more important for two reasons. It is generally believed that the noisiness of the avalanche diode will be the ultimate limitation to its applications and its major weakness in comparison with other microwave sources. Second, its large noise generation makes the avalanche diode an attractive noise source for microwave frequencies.[1]

The present investigation will be both experimental and theoretical in nature. The experimental study will include the measurement of the noise figures of avalanche-diode amplifiers, and the AM and FM noise output of avalanche diode oscillators under different operating conditions, particularly at large-signal levels. The noise performance will be related to operating and circuit conditions, diode parameters and semiconductor material properties. The noise generation mechanisms in an avalanche diode will be studied analytically in order to explain the experimentally observed results and a noise model for the diode will be developed. The analysis will include the effects of spontaneous fluctuations in the ionization rate and investigation of the noise behavior under large-signal operating conditions.

8.2 Experimental Noise Evaluation Circuit. An RF test circuit was fabricated during this period for experimental studies. It consists of an avalanche diode mounted in a 50-Ω coaxial cavity with sliding tuning slugs, a heat sinking arrangement for the diode and provision for cooling to liquid nitrogen temperature. A computer program for evaluating such a circuit was developed earlier under this project.[2]

1. Haitz, R. H. and Opp, F. L., "A Solid State Broad-Band Microwave Noise Source," Presented at the IEEE Int. Electron Devices Meeting, Washington, D. C., October 1968.

2. Haddad, G. I. et al., "Microwave Device Investigations," Semiannual Progress Report No. 6, Electron Physics Laboratory, The University of Michigan, Ann Arbor, p. 21, October 1969.

8.3 Calculation of Noise Parameters. The avalanche-diode amplifier may be considered a linear device for small signals, and as such its noise behavior may be characterized by four noise parameters.[3] They can be evaluated by measuring the noise figure as a function of source admittance. A general and widely applicable computer program has been developed to carry out this evaluation. The "best fit" noise parameters are estimated by the method of steepest descent which is used to reduce a chosen error norm. Several options are available in the program concerning choice of error criteria, units of input data, assignment of confidence weights to measurements and automatic rejection of measurements. Since it is of general utility, this program, accompanied by a detailed documentation, is being submitted for publication to a journal.

8.4 Program for the Next Period. Measurements will be made on the fabricated circuit and the circuit will be used to design an avalanche-diode amplifier for the measurement of the noise figure. Effects of temperature and signal level will be observed. The computer program described above will be used for the computation of noise parameters. The minimum noise figures thus calculated and the noise measure of the amplifier[4] will be used as the common basis for the comparison of noise performance under various operating conditions. A nonlinear theory to explain the excessive noise above a threshold signal level (in the case of avalanche-diode amplifiers) and a threshold dc bias current (in the case of avalanche-diode oscillators)[5] will be developed.

---

3. "IRE Standards on Methods of Measuring Noise in Linear Twoports, 1959," Proc. IRE, vol. 48, No. 1, pp. 60-68, January 1960.

4. Haus, H. A. and Adler, R. B., Circuit Theory of Linear Noisy Networks, Technology Press of M.I.T., Cambridge, Mass., p. 4, 1959.

5. Cowley, A. M., Fazarinc, Z., Hall, R., Hamilton, S., Yen, C. and Zettler, R., "The Singly-Tuned IMPATT Oscillator," IEEE Int. Solid State Circuits Conference Digest, Philadelphia, Penn., pp. 10-11, February 1970.

9. Metal-Oxide-Metal Detectors

Supervisor: G. I. Haddad

Staff: S. P. Kwok

9.1 Introduction. The second-order asymmetry in the I-V characteristics of the metal-(insulator/oxide)-metal, M-I-M/M-O-M, structure with two dissimilar metal electrodes can be used for signal detection without bias.[1] Thornber et al.[2] and Lewicke and Mead[3] measured and extrapolated the RC time constant of Al-AlN-Mg and Al-AlN-Al structures with an insulator thickness of 10 Å to be about 10^{-12} s. Experimentally, Hocker et al.[4] and Green[5] observed frequency mixing of the HCN, 337-μm laser line with the thirteenth harmonic of a V-band klystron using a point-contact M-O-M structure, thus showing the RC time constant to be on the order of 10^{-12} s or smaller. The simplicity of the structure and its capability for room temperature detection of millimeter-, submillimeter- and shorter wavelength signals, prompted a more detailed study of the detection properties of the M-O-M detector during this period. A different approach was used to derive the detection characteristics of the M-O-M structure. The results agree well with those of Green.[5] More exact calculations were performed on a computer; the results predict well both the small-signal and large-signal characteristics.

---

1. Coleman, P. D. and Green, S. I., "A Fast, Room Temperature, Millimeter and Submillimeter Electric-Tunnel Effect Detector," Presented at the IEEE Int. Electron Devices Meeting, Washington, D. C., October 1968.

2. Thornber, K. K., McGill, T. C. and Mead, C. A., "The Tunneling Time of an Electron," J. Appl. Phys. (Correspondence), vol. 38, No. 5, pp. 2384-2385, April 1967.

3. Lewicke, C. and Mead, C. A., "Experimental Determination of E-k Relationship in Electron Tunneling," Phys. Rev. Letters, vol. 16, No. 21, pp. 939-941, 23 May 1966.

4. Hocker, L. O., Sokoloff, D. R., Daneu, V., Szoke, A. and Javan, A., "Frequency Mixing in the Infrared and Far-Infrared Using a Metal-to-Metal Point Contact Diode," Appl. Phys. Letters, vol. 12, No. 12, pp. 401-402, 15 June 1968.

5. Green, G. I., "A Point Contact Electric Tunneling Detector for Millimeter and Submillimeter Waves," Ph.D. Thesis, University of Illinois, 1969.

9.2 Small-Signal Detection Theory.

9.2.1 Small-Signal I-V Characteristic.

Using an idealized trapezoidal barrier as shown in Fig. 9.1, the tunneling current at T = 0°K may be expressed as

$$I = I_o\left(\int_0^{\eta-eV} (eV)D(E_x)dE_x + \int_{\eta-eV}^{\eta} (\eta - E_x)D(E_x)dE_x \right), \tag{9.1}$$

where $D(E_x)$ = probability of transmission = $-4\pi/h \int_{S_1}^{S_2} \{2m[U(x) - E]\}^{1/2}\, dx$ (WKB approximation),

$I_o = 4\pi me/h^3$,

m = electron mass,

h = Planck's constant,

η = Fermi energy,

V = applied voltage,

$E_x = (1/2)\, mv_x^2$,

v_x = the longitudinal velocity component and

U(x) = the potential barrier.

S_1, S_2 are the classical turning points in tunneling. For small eV the above expression can be expanded as

$$I = I_o\left(a_1(eV) + a_2(eV)^2 + a_3(eV)^3\right) \tag{9.2}$$

and

$$D(E_x) = A_o(E_x) + A_1(E_x)(eV) + A_2(E_x)(eV)^2 \quad . \tag{9.3}$$

The current density can be calculated to be

$$I_{F,R} = \frac{1}{R}\left(V + g_{2F,R}\, V^2 + g_{3F,R}\, V^3\right) , \tag{9.4}$$

where

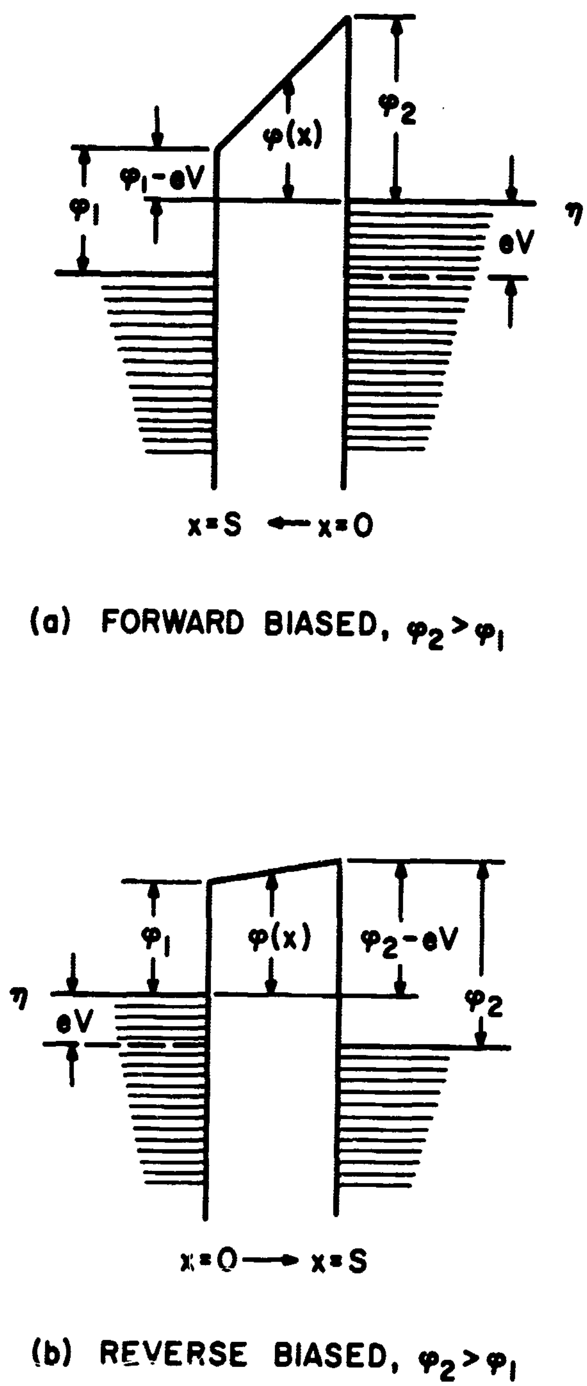

FIG. 9.1 TRAPEZOIDAL BARRIER OF THE M-O-M STRUCTURE.

$$R = \frac{D^2 e^D h^3}{8\pi m e^2 \varphi_o (D+1)} \frac{1}{a} , \qquad (9.5)$$

$$\mathcal{E}_{2F,R} = \pm \frac{\alpha D^2}{12} \left(\frac{e}{2\varphi_o} \right) \left(1 + DE_i(-D) e^D \right) , \qquad (9.6)$$

$$\mathcal{E}_{3F,R} = \frac{D^2}{24} \left(\frac{e}{2\varphi_o} \right)^2 \left(1 + \frac{DE_i(-D) e^D}{2} \right) , \qquad (9.7)$$

$$D = 1.023 \left(\frac{\varphi_o}{e} \right)^{1/2} \hat{S} , \qquad (9.8)$$

$$\varphi_o = \frac{\varphi_1 + \varphi_2}{2} ,$$

$$\alpha = \frac{\varphi_2 - \varphi_1}{\varphi_2 + \varphi_1} ,$$

$$E_i(-D) = \int_{\infty}^{D} \frac{e^{-t}}{t} dt ,$$

φ_i = the work function of the ith metal,

$\hat{S}$ = the insulator thickness in Å and

a = the contact area in m^2.

The subscripts F,R and signs ± correspond to forward and reverse biases, respectively. Forward bias is defined as positive bias on the metal with a lower work function.

9.2.2 Small-Signal Detection. When a small input signal $V = V_o \sin\theta$ is applied across the M-O-M structure, the detected dc voltage across the structure is given by:

$$\Delta V = \Delta IR = \frac{1}{2\pi} \int_0^{\pi} (g_{2F} - g_{2R})V^2 \, d\theta + \int_0^{\pi} (g_{3F} - g_{3R})V^3 \, d\theta \quad , \tag{9.9}$$

which can be reduced to

$$\Delta V = \frac{\alpha D^2}{48} \left(\frac{e}{\varphi_o} \right) \left(1 + DE_i(-D)e^D \right) V_o^2 \quad . \tag{9.10}$$

It is clear that for small-signal levels,

$$V_o \ll \frac{4 \left(\frac{\varphi_o}{e} \right)^{1/2}}{\hat{S}} \quad , \tag{9.11}$$

where φ_o/e is in electron volts and V_o is in volts. The M-O-M structure is a square-law detector and this will be seen in the experimental results presented later.

For practical structures $\hat{S} \geqq 10$ (Å), so $D \geqq 10$ and $1 + DE_i(-D)e^D \approx 1/D$ and the resistance simplifies to

$$R \approx 3.069 \times 10^{-15} \frac{\hat{S}}{\left(\frac{\varphi_o}{e} \right)^{1/2}} \frac{1}{a} \exp \left[1.023 \, \hat{S} \left(\frac{\varphi_o}{e} \right)^{1/2} \right] \quad , \tag{9.12}$$

$$RC \approx 2.72 \times 10^{-16} \frac{\epsilon_r}{\left(\frac{\varphi_o}{e} \right)^{1/2}} \exp \left[1.023 \, \hat{S} \left(\frac{\varphi_o}{e} \right)^{1/2} \right] \tag{9.13}$$

and

$$C = \frac{\epsilon_o \epsilon_r a}{S} \quad , \tag{9.14}$$

where ϵ_o = the vacuum permittivity,

ϵ_r = the relative dielectric constant and

S = the insulator thickness in m.

The responsivity of the M-O-M detector is defined as

$$\gamma = \frac{\text{detected voltage}}{\text{input power}} = \frac{\Delta V}{\left(\frac{V_o^2}{2R}\right)}$$

and can be expressed as

$$\gamma \approx 1.31 \times 10^{-16} \frac{\hat{S}^2 \alpha}{a\left(\frac{\varphi_o}{e}\right)} \exp\left[1.023\, \hat{S} \left(\frac{\varphi_o}{e}\right)^{1/2}\right] . \tag{9.15}$$

The responsivity-bandwidth product is given by

$$\frac{\gamma}{2\pi RC} = 7.66 \times 10^{-2} \frac{\hat{S}^2 \alpha}{a\epsilon_r \left(\frac{\varphi_o}{e}\right)^{1/2}} . \tag{9.16}$$

It is interesting to note that the RC time constant is independent of the contact area. The bandwidth increases rapidly with decreasing insulator thickness while the responsivity decreases. It is desirable to have a small contact area for increasing responsivity without trading off bandwidth. The plots of bandwidth, responsivity and responsivity-bandwidth product as functions of device parameters are given in Figs. 9.2, 9.3 and 9.4, respectively.

9.3 Experiment. A polished metal or a metal thin film on the order of 2000 Å evaporated on a piece of glass plate was used as the first metal electrode. The metals used were Al, Tn and Au. The naturally grown oxide on the surface constitutes the insulator. W and Be-Cu whisker wires which were electroetched to form a sharp tip with a diameter dimension on the order of 1 μm were used as the second electrode. Figure 9.5 shows the detector mounted in a waveguide. The presence of a micrometer screw allows adjustment of the whisker pressure. At first the whisker is made to contact

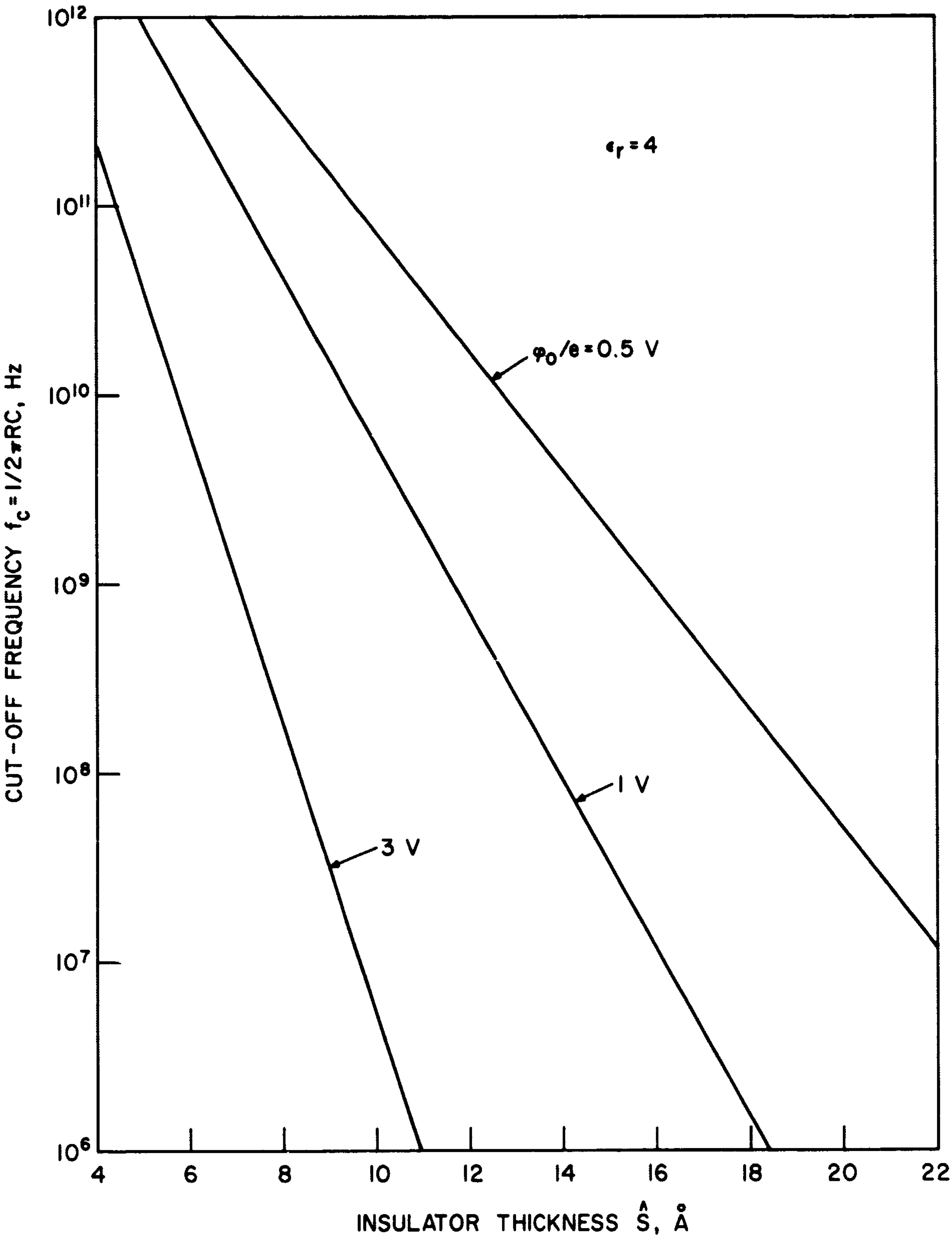

FIG. 9.2 CUT-OFF FREQUENCY VS. INSULATOR THICKNESS, WHERE $f_c = 5.85 \times 10^{14} \cdot [(\varphi_o/2)^{1/2}/\epsilon_r] \exp [-1.023\, \hat{S}(\varphi_o/e)^{1/2}]$ (Hz).

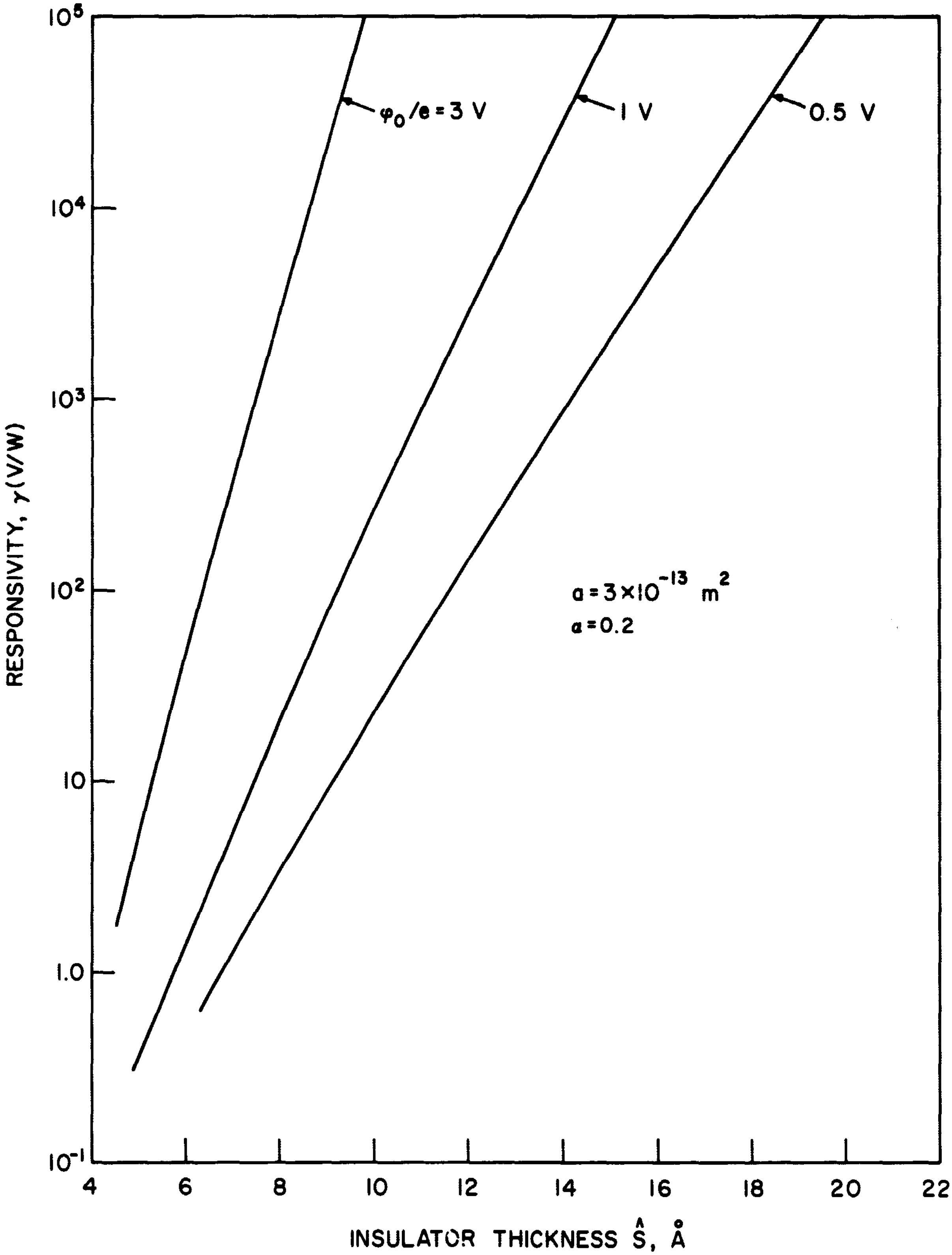

FIG. 9.3 RESPONSIVITY VS. INSULATOR THICKNESS, WHERE $\gamma = 1.31 \times 10^{-16} \cdot [\hat{S}^2 \alpha/a(\varphi_o/e)] \exp [1.023\ \hat{S}(\varphi_o/e)^{1/2}]$.

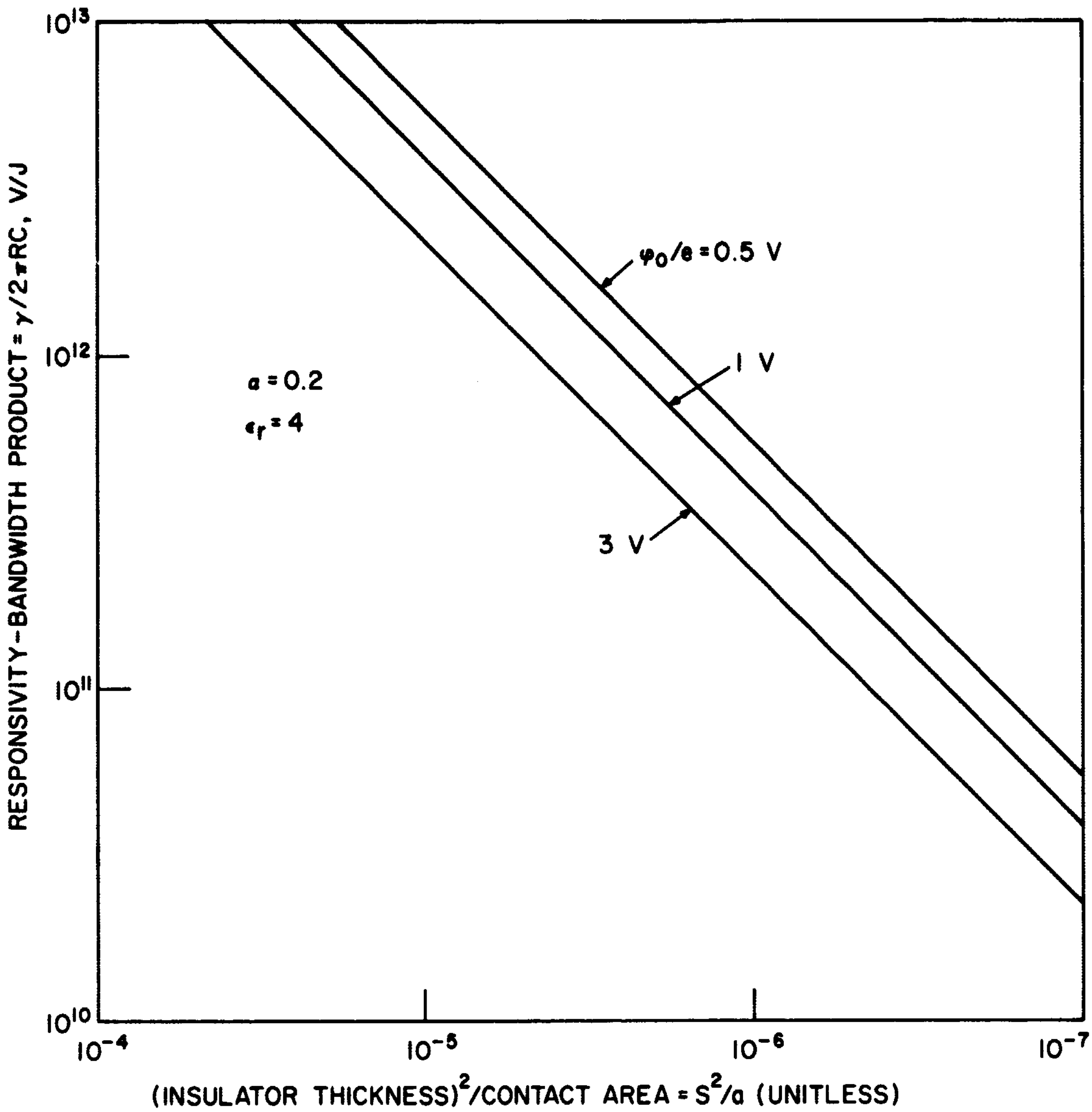

FIG. 9.4 RESPONSIVITY-BANDWIDTH PRODUCT VS. (INSULATOR THICKNESS)^2/CONTACT AREA, WHERE $\gamma/2\pi RC = 7.66 \times 10^8\,[\alpha/\epsilon_r(\varphi_o/e)^{1/2}](S^2/a)$ (V/J).

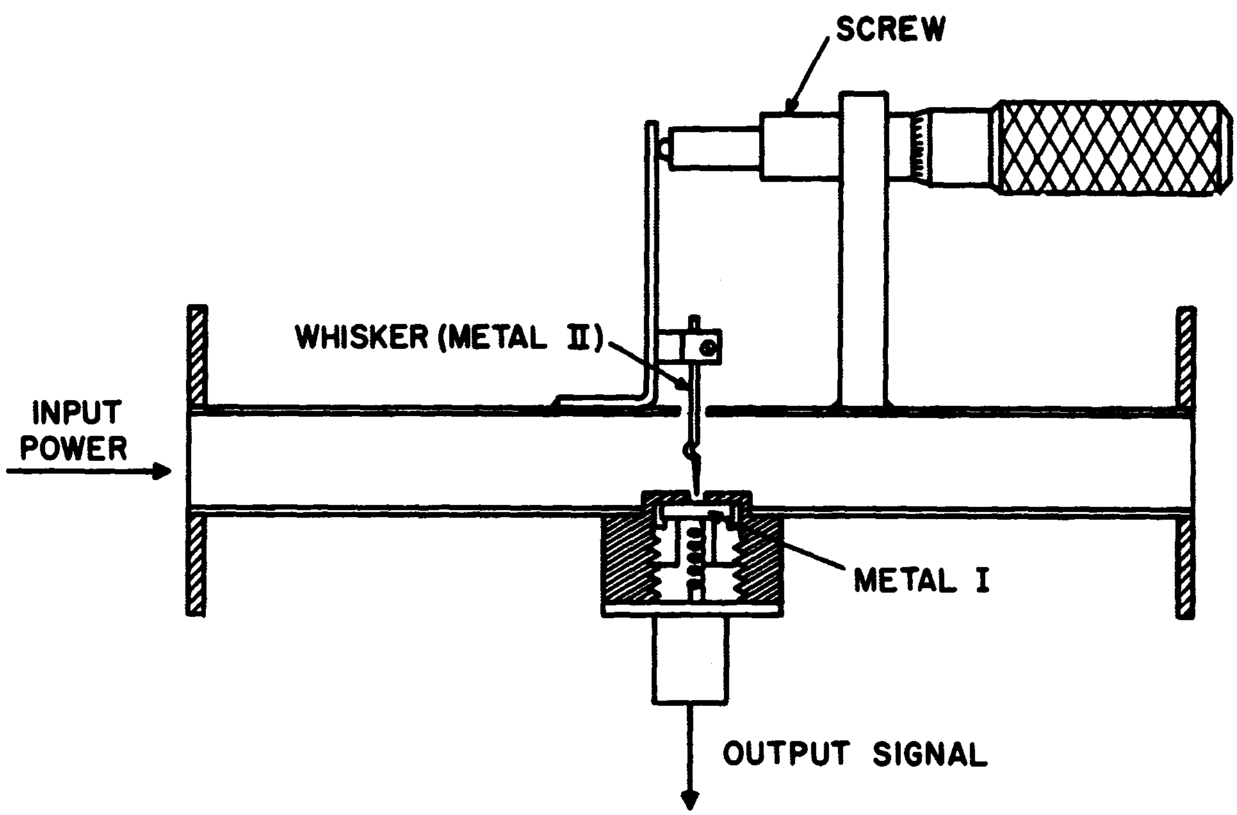

FIG. 9.5 M-O-M DETECTOR WAVEGUIDE MOUNT.

the film by adjusting the micrometer then the whisker pressure is released slowly. The best detector performance occurs when the whisker is just about to separate from the insulating film. Figure 9.6 shows the complete experimental setup. The pulse sweep circuit was connected to the M-O-M diode to observe the I-V characteristics with or without the microwave power applied without dismantling the setup. Good care must be taken to avoid mechanical vibration and excessive dc power dissipation, both of which may alter or permanently damage the diode. The responsivity of a M-O-M diode is given in Fig. 9.7. At low-signal levels the diode is a square-law detector but at higher levels the cubic term becomes dominant.

Polarity reversal of the detected signal may occur at a large-signal level. Figure 9.8 shows the responsivity of two diodes with different values of resistance. Polarity reversal is often accompanied by an unstable detected output signal. In some devices no such phenomenon was observed, e.g., Fig. 9.7 but presumably the polarity would reverse at a higher power level.

9.4 Polarity Reversal. The small-signal theory based on a trapezoidal barrier model does not predict polarity reversal at large-signal levels. If a slight perturbation on the trapezoidal barrier is included as an effect of the image potential, and using the model shown in Fig. 9.9, the following expression for detected voltage is obtained:

$$\Delta V = \frac{\alpha D}{48}\left(\frac{e}{\varphi_o}\right)\left[1 + \frac{3}{10} D\left(\frac{\beta}{\varphi_o}\right)\right] V_o^2 \left(1 - \frac{V_o}{V_{or}}\right) , \tag{9.17}$$

where

$$V_{or} = \frac{3\pi}{8}\left(\frac{g_{2F} - g_{2R}}{g_{3R} - g_{3F}}\right) = \frac{5\pi}{2}\left(\frac{\varphi_o}{\beta}\right)\left(\frac{\varphi_o}{e}\right)\left[1 + \frac{3}{10} D\left(\frac{\beta}{\varphi_o}\right)\right]\frac{1}{D} \tag{9.18}$$

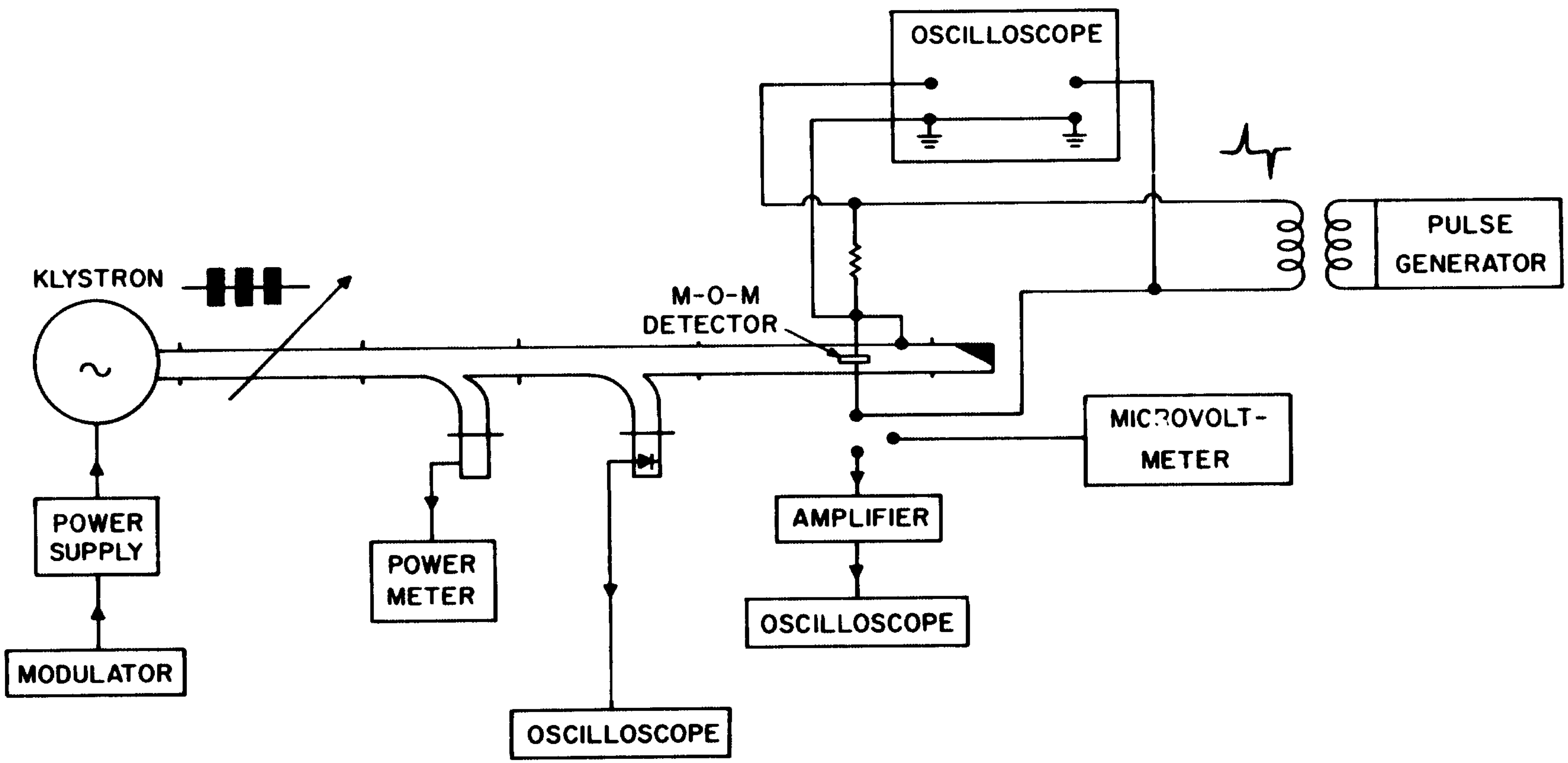

FIG. 9.6 EXPERIMENTAL SETUP FOR THE M-O-M DETECTOR.

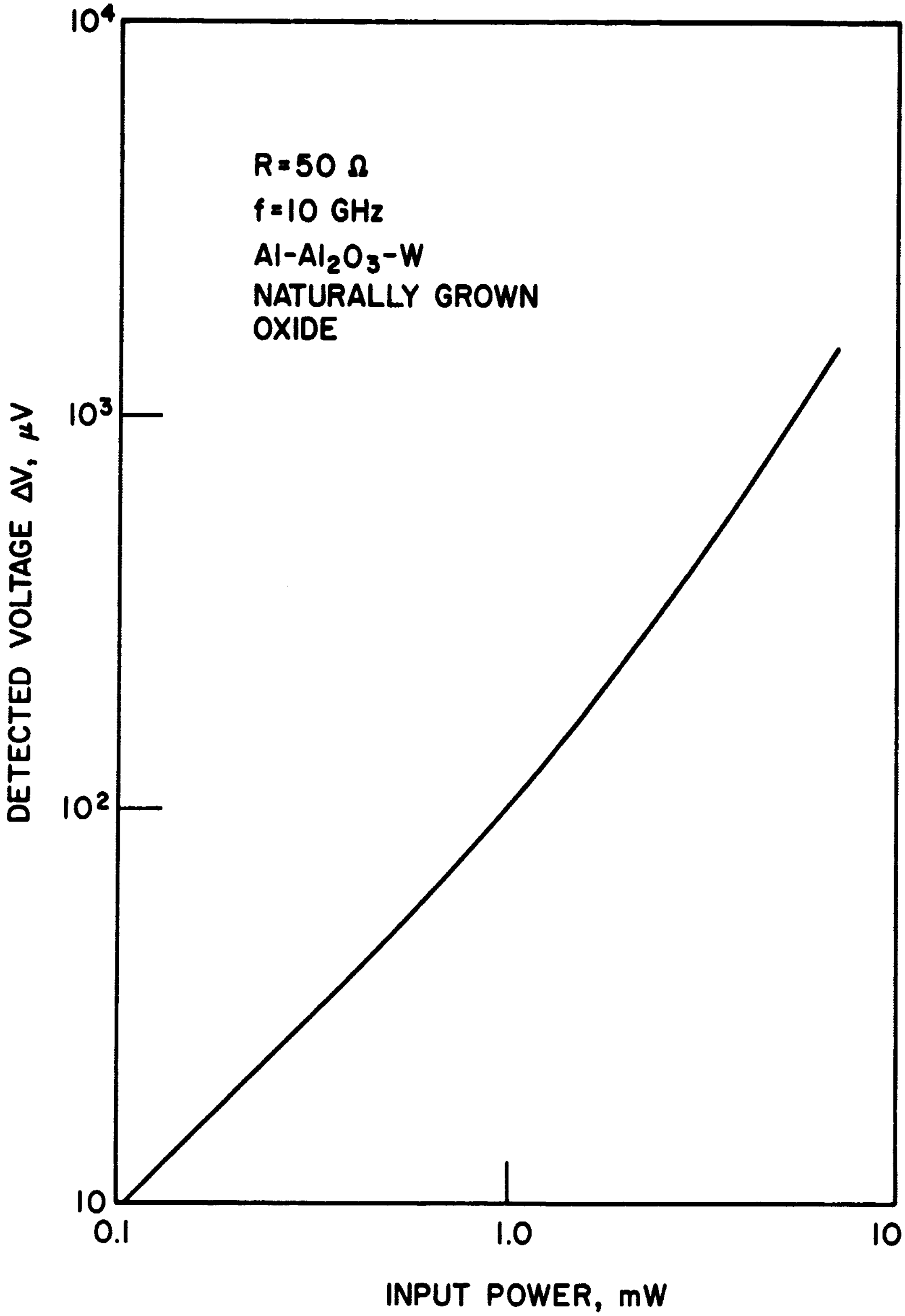

FIG. 9.7 RESPONSIVITY OF A M-O-M DIODE.

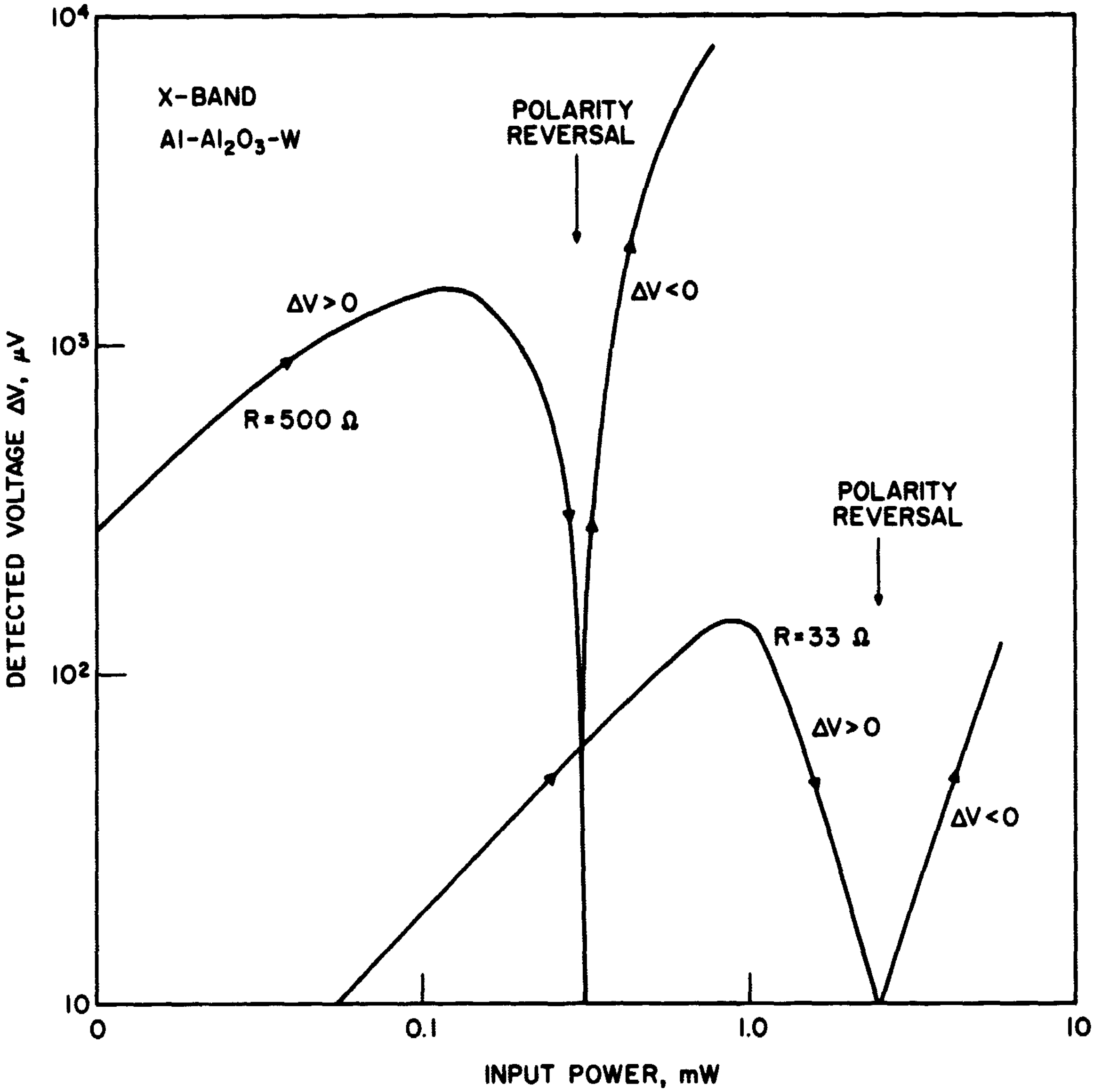

FIG. 9.8 RESPONSIVITY AND POLARITY REVERSAL.

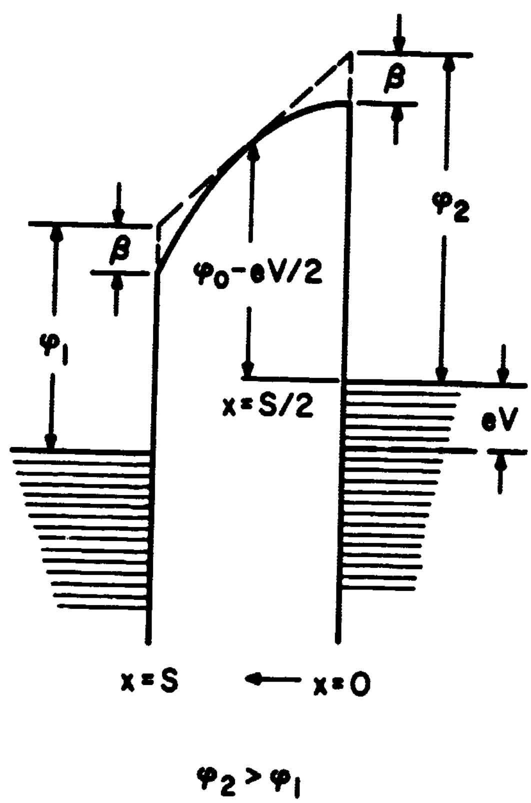

FIG. 9.9 PERTURBED TRAPEZOIDAL BARRIER.

and β = perturbation potential (Fig. 9.9). For a small perturbation, $D(\beta/\varphi_o) \leq 1$, V_{or} simplifies approximately to

$$V_{or} = \frac{5\pi}{2}\left(\frac{\varphi_o}{\beta}\right)\left(\frac{\varphi_o}{e}\right)\frac{1}{D} \quad . \tag{9.19}$$

Polarity reversal occurs at a signal voltage of about $(5\pi/2)(\varphi_o/e)$ or higher, which is about five times higher than that obtained later by more exact computer calculation. Moreover, at such high signal levels the small-signal analysis breaks down.

9.5 More Exact Computer Calculation of I-V Characteristics. In view of the deviation of the detection property from the square law and the occurrence of large-signal polarity reversal a more exact numerical calculation which includes the effect of the image potential was carried out by a computer. Using the approximation of image potential due to Simmons,[6]

$$\varphi_i = -1.15\left(\frac{e^2 \ln 2}{8\pi\epsilon_o\epsilon_r S}\right)\frac{S^2}{x(S - x)} \quad , \tag{9.20}$$

we obtain the I-V characteristics of the M-O-M diode with different barrier thicknesses and dielectric constants as shown in Fig. 9.10. The I-V characteristics exhibit a second-order asymmetry which becomes increasingly marked at a larger voltage level. The image potential reduces both the barrier height as well as the width, thus increasing the current

6. Simmons, J. G., "Generalized Formula for the Electric Tunnel Effect Between Similar Electrodes Separated by a Thin Insulating Film," J. Appl. Phys., vol. 34, No. 6, pp. 1793-1803, June 1963.

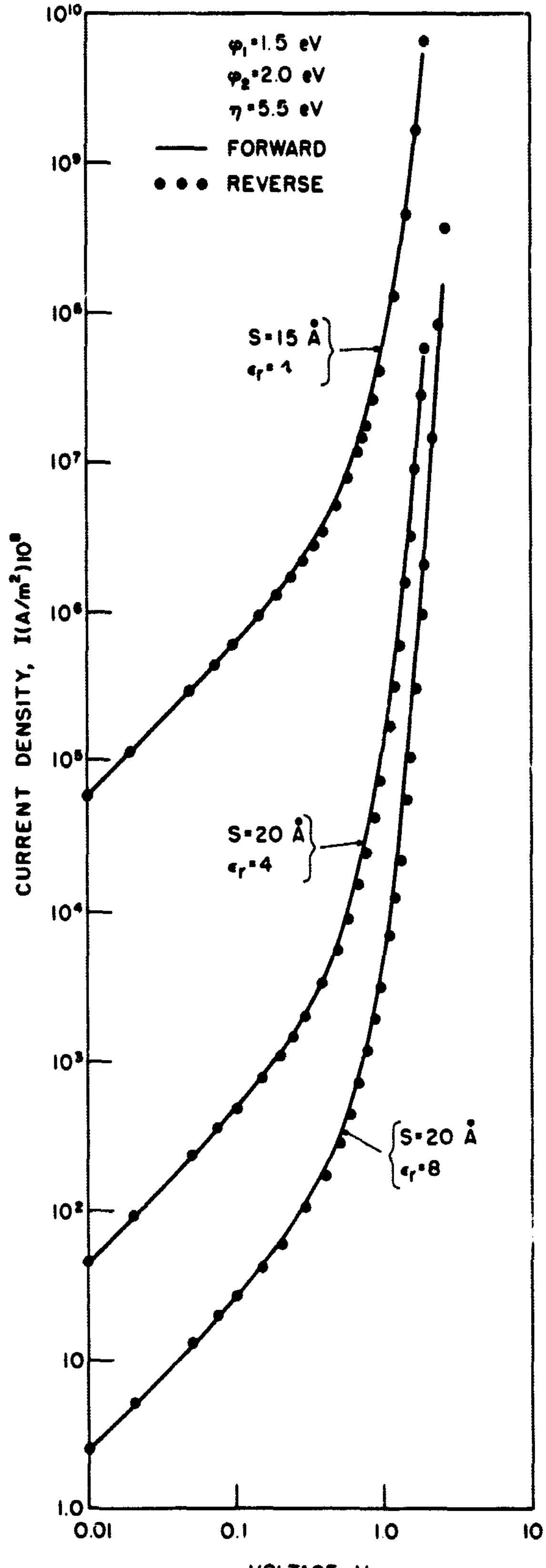

FIG. 9.10 I-V CHARACTERISTICS OF M-O-M DIODES.

density. Through the expression of image potential it is seen that the increase in dielectric constant reduces current density.

9.6 Detected Current Density. The detected current density can be expressed as

$$\Delta I = \frac{1}{2\pi}\left(\int_0^{\pi} I_F(V_o \sin\theta)\,d\theta - \int_0^{\pi} I_R(V_o \sin\theta)\,d\theta\right) . \qquad (9.21)$$

The parentheses indicate the functional dependence of current density on V_o and θ. The plot of detected current vs. the applied peak voltage is shown in Fig. 9.11. At small-signal levels the detector obeys approximately a square law, however it deviates from the latter proportionately as the signal level increases. The polarity reversal occurs at a voltage level close to the value φ_2/e (the larger work function). A decrease in dielectric constant decreases the voltage at which polarity reverses. Thus the image potential enhances the occurrence of polarity reversal at lower voltage, though not as significantly as the effect of φ_2. As experimentally shown in Fig. 9.8, polarity reverses at a lower input power level for the device with a higher resistance value. This point can be seen from $P = V_{or}^2/2R$, where $V_{or} \sim \varphi_2/e$ is relatively constant while R changes widely. Hence higher resistance devices tend to reverse polarity at lower power levels. Quantitatively, from the experiment (Fig. 9.8), polarity reverses at $V_{or} \sim 0.5$ V whereas the predicted value $\varphi_2/e \sim 1$ or 2 V.

The marked increase of the detected current density from the square-law characteristics is not as significantly reflected as on the responsivity observed experimentally (Figs. 9.7 and 9.8). The resistance of the M-O-M structure is known to decrease rapidly with an increase in the dc current, hence countering the effect of the former on the detected voltage. Another

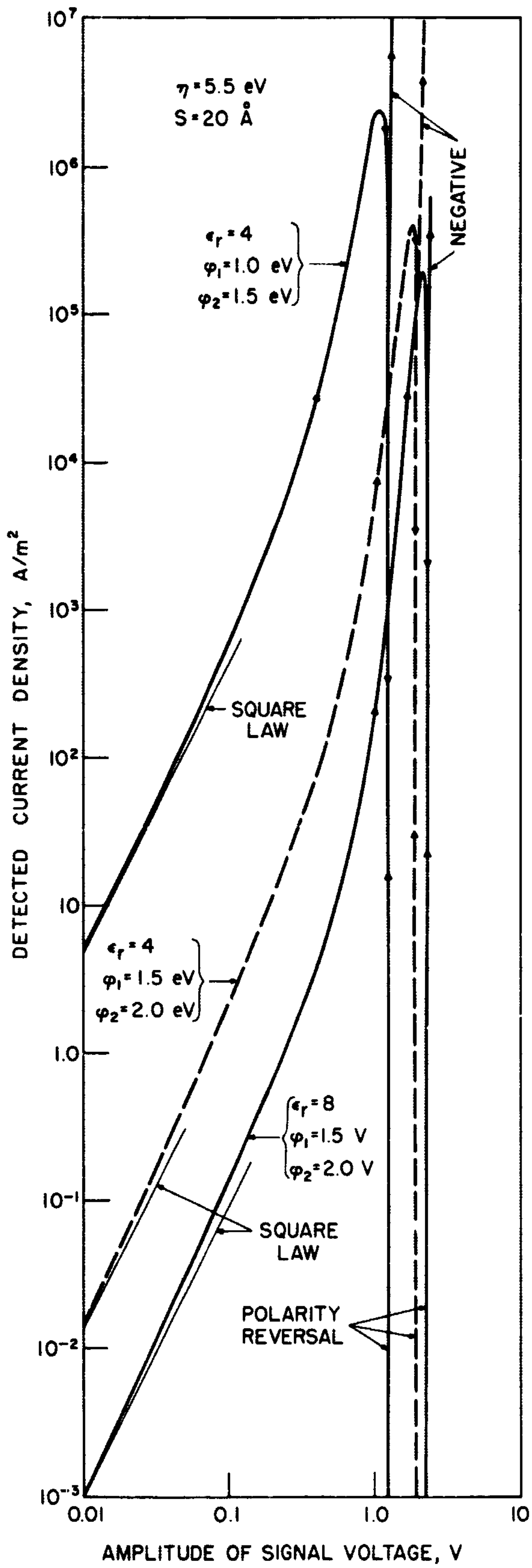

FIG. 9.11 RESPONSIVITY OF M-O-M DIODES.

detection scheme which measures the current instead of the voltage across the diode should agree better with the calculations.

9.7 Conclusions. Small-signal calculations of the I-V characteristic and the detection properties of the M-O-M structure using an idealized trapezoidal barrier by the expansions of the transmission probability,

$$D(E_x) = A_0(E_x) + A_1(E_x)(eV) + A_2(E_x)(eV)^2$$

and

$$I = I_0\left(a_1(eV) + a_2(eV)^2 + a_3(eV)^3\right) ,$$

yield results which are in good agreement with the work of Green,[5] who used the generalized I-V relation due to Simmons.[6-8] The small-signal theory predicts the M-O-M structure to be a square-law detector which agrees fairly well with the observed characteristics at small-signal levels. Moreover, the analyses reveal the essential detector characteristics such as: bandwidth, responsivity and responsivity-bandwidth product as functions of the device parameters: work function of the metals, thickness of the insulating film, the dielectric constant of the film and the area of point contact. No attempt was made to perform calculations at $T \neq 0°K$, since the thermal effect on the I-V characteristics[8] will not change significantly for room temperature operation.

---

7. Simmons, J. G., "Electric Tunnel Effect Between Dissimilar Electrodes Separated by a Thin Insulating Film," J. Appl. Phys., vol. 35, No. 8, pp. 2472-2481, August 1964.

8. Simmons, J. G., "Generalized Thermal J-V Characteristics for the Electric Tunnel Effect," J. Appl. Phys., vol. 35, No. 9, pp. 2655-2658, September 1964.

The above small-signal analysis precludes polarity reversal. However, if a slight perturbation is introduced on the trapezoidal barrier as an artificial image potential, the calculation shows the possibility of large-signal reversal though the quantitative prediction is inadequate.

Finally, the computer calculation of the detected current explains the deviation of the responsivity from that of a square law. The large-signal polarity reversal was estimated to occur when the applied voltage is close to φ_2/e, φ_2 being the higher work function of the two metals. The value estimated is on the same order of magnitude as that observed experimentally. The polarity reversal for a higher resistance diode occurring at a lower power level was also explained from the results of the above calculations.

9.8 Program for the Next Period. This phase of the program has been concluded and a technical report on this work is presently being prepared and will be available in the near future.

10. High-Frequency Limitations of Avalanche-Diode Oscillators

Supervisor: G. I. Haddad

Staff: S. P. Kwok

10.1 Introduction. The operating frequency of an avalanche-diode oscillator of the type p^+nn^+ is approximately related to the width of the n-type region as $\omega = \pi v/W$, where v is the carrier saturated drift velocity and W is the width of the n-region. For high-frequency operation of the oscillator it is necessary to make the n-region narrow and eventually at higher frequencies to dope the n-region moderately heavily in order to achieve optimum performance. If the field thus created is high enough a significant amount of electrons could tunnel from the valence band of the p^+-region to the conduction band of the n-region, and then drift to the n^+-region under the influence of the electric field. Unlike avalanche multiplication where there is an inherent $\pi/2$ phase lag of current relative to the field due to the nature of ionization buildup,[1] the tunneling current phase lag determined by the tunneling transition time is believed to be small. The bulk of the phase delay necessary to produce a negative resistance must come from the transit time in the narrow n-region. This may constitute a high-frequency limitation on the power output of the oscillator.

10.2 Program Status. Presently a computer calculation of tunneling current in a p^+n junction for various doping levels and n-region widths is underway in order to determine the conditions when the tunneling current becomes significant.

The transit time of electron tunneling has been investigated. It was shown[2] that this transit time is dependent on the junction width and the transmission coefficient phase factor as

$$t = \frac{\ell}{V_v} + \mathrm{Im}(\ell n\ \tau) \quad . \tag{10.1}$$

where ℓ = the junction width,

V_v = the electron velocity in the valence band,

τ = the transmission coefficient of tunneling and

Im = the imaginary part.

It was also found that the tunneling current in general is highly dependent on the width of the potential barrier, e.g., a detailed study of the I-V characteristic of the M-O-M structure (see Section 9) shows an

1. Read, W. T., "A Proposed High-Frequency Negative-Resistance Diode," Bell System Tech. J., vol. 37, No. 2, pp. 401-446, March 1958.

2. Fredkin, D. R. and Wannier, G. H., "Theory of Electron Tunneling in Semiconductor Junctions," Phys. Rev., vol. 128, No. 5, pp. 2054-2061, 1 December 1962.

exponential dependence of current on the barrier width. For a certain doping profile the band structure of a p^+nn^+ diode is shown in Fig. 10.1 where significant tunneling only occurs in the small region $x \leq \ell$. Upon reaching the conduction band of the n-region electrons drift to the n^+-region. If a proper phase delay is achieved, power may be delivered. The transit time of tunneling is finite but in general is different from the $\pi/2$ phase delay due to avalanche multiplication. It is therefore expected that when the space-charge layer becomes very narrow tunneling may play an important role in determining the power output which can be achieved.

10.3 Program for the Next Period. Quantitative calculations of the tunneling current densities for various doping levels and base widths of reverse-biased p^+n junctions will be performed. These will aid in determining the relative magnitude of the currents due to tunneling and avalanche breakdown and also the distribution of the tunneling electrons appearing in the drift region.

11. Superconducting Junctions for Millimeter-Wave Detection

Supervisor: G. I. Haddad

Staff: H. Ando

11.1 Introduction. Superconducting junctions, which are formed by having two superconducting metals separated by a thin layer of dielectric, show excellent promise in applications as detectors, mixers and self-oscillating mixers in the millimeter- and submillimeter-wave region of the electromagnetic spectrum. These junctions can respond to radiation in a broad region about their superconducting energy gap, are highly sensitive and respond at high speeds. The superconducting energy gap E_g of some common superconductors are listed below:

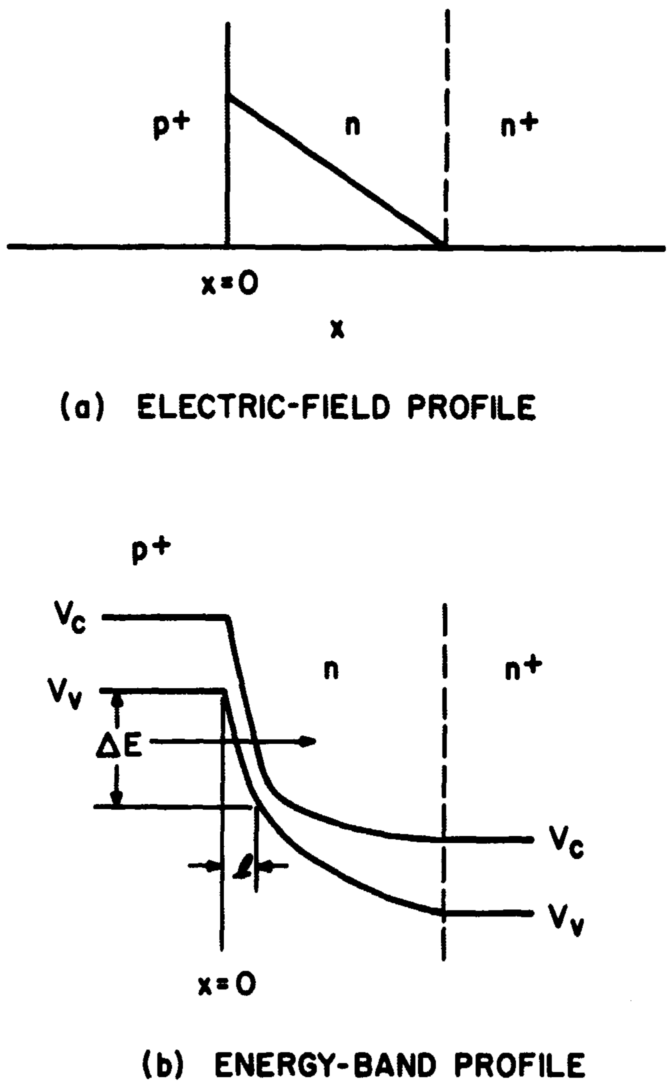

FIG. 10.1 ELECTRIC-FIELD AND ENERGY-BAND PROFILES OF A p^+nn^+ DIODE.

$E_g(Al) = 76.6$ GHz , $E_g(In) = 251$ GHz , $E_g(Sn) = 266$ GHz ,
$E_g(Ta) = 335$ GHz , $E_g(Hg) = 395$ GHz , $E_g(Pb) = 642$ GHz ,
$E_g(Nb) = 728$ GHz .

More materials are continually being discovered to have superconducting properties, and as such, may some day be added to the list of possible detector materials. It has been shown by Bardeen et al.[1] that when a superconducting material is cooled below a certain critical temperature T_c it becomes more favorable for the electrons in the material to pair up with one another rather than to remain as single electrons as in ordinary metals. Thus a superconducting current consists of a flow of these electron pair couplets (called Cooper pairs) rather than single electrons, and superconducting tunneling through a dielectric barrier consists of Cooper pair tunneling rather than electron tunneling. If there is a nonzero potential difference V between the two superconducting metals across the dielectric barrier, Cooper pairs on different sides of the barrier will have energies differing by $\Delta E = 2$ eV. Tunneling through such a barrier can then take place only as a virtual process. From quantum mechanics it is known that in such a system there are oscillating currents at a frequency $f = \Delta E/\hbar$, i.e., $f = 2\ eV/\hbar$. When the interaction between the oscillating currents and the electromagnetic field is taken into account, it is found that real processes can take place if energy is conserved by the emission of a photon of the correct frequency. In this case the radiation will be coherent since every photon comes from an identical process. Thus if electromagnetic radiation is applied to the barrier from an external microwave source at the same frequency as the oscillating supercurrents, then energy can be transferred in

1. Bardeen, J., Cooper, L. N. and Schrieffer, J. R., "Theory of Superconductivity," Phys. Rev., vol. 108, No. 5, pp. 1175-1204, December 1957.

either direction depending on the phase relationship between the two systems, provided the two oscillating systems are coupled together. For this type of coupling to be strong it is necessary that both the oscillating supercurrents and the electric field in the barrier produced by the microwave radiation be in phase over all of the barriers, hence smaller barriers are more favorable than larger ones for coupling these two types of systems.

Thus it is seen that under the proper conditions microwave radiation can induce the transfer of Cooper pairs across a superconducting junction and that this also can occur at certain nonzero potential differences across the barrier, provided that energy is conserved, i.e., $f = 2\,eV/\hbar$, where f = the frequency of the external microwave radiation and V = the potential difference across the barrier. It is precisely this aspect of how applied external microwave radiation induces the transfer of superconducting Cooper pairs across the junction which is of interest in detector and mixer applications.

11.2 Work During This Period. During this period some of the theoretical aspects of the superconducting junction which will be needed for the detection schemes have been investigated; namely, the tunneling supercurrent and its variation with frequency and with changes in applied microwave power have been considered.

The fact that the tunneling supercurrent should vary with a Bessel function dependence with applied microwave power was first pointed out by Josephson[2] in his original paper predicting such supercurrent tunneling. Shapiro et al.[3] have derived a phenomenological expression for this dependence as

---

2. Josephson, E. D.,"Possible New Effects in Superconductive Tunnelling," Phys. Letters, vol. 1, No. 7, pp. 251-253, July 1962.

3. Shapiro, S., Janus, A. R. and Holly, S., "Effect of Microwaves on Josephson Currents in Superconducting Tunneling," Rev. Mod. Phys., vol. 36, No. 1, pp. 223-225, January 1964.

$$I_s = I_o \sum_{n=o}^{\infty} J_n \left(\frac{2\ ev}{\hbar f} \right) \left(\cos(\omega + np)t + (-1)^n \cos(\omega - np)t \right) ,$$

where I_s = the tunneling supercurrent,

I_o = the maximum supercurrent at zero dc bias voltage,

v = the amplitude of the applied microwave voltage across the junction,

f = the frequency of the applied microwave radiation,

ω = $2\ eV/\hbar$ is the angular frequency of the alternating supercurrent,

V = the dc bias voltage across the junction and

p = $2\pi f$.

Thus it is seen that the amplitude of the dc supercurrent is given by the term n = 0 and varies as J_o, the zero-order Bessel function. This is the tunneling current which occurs at zero dc bias. However the above equation gives no detailed information about I_o. To obtain this dependence the more detailed derivation of Werthamer[4] was used. He derives the following expression for the dc supercurrent:

$$I_{dc} = \text{Im} \sum_n \left\{ J_n^2 \left(\frac{ev}{\hbar f} \right) j_1 \left[\left(n - \frac{1}{2} N \right) f \right] + J_{N-n} \left(\frac{ev}{\hbar f} \right) J_n \left(\frac{ev}{\hbar f} \right) e^{j\alpha} \cdot j_2 \left[\left(n - \frac{1}{2} N \right) f \right] \right\} ,$$

where α = a phase factor and

j_1, j_2 = complex expressions dependent on f and E_g.

4. Werthamer, N. R., "Nonlinear Self-Coupling of Josephson Radiation in Superconducting Tunnel Junctions," Phys. Rev., vol. 147, No. 1, pp. 255-263, July 1966.

For N = 0 the analogous term for n = 0 is found in the Shapiro treatment.[3] During this period a computer program was written to evaluate the expression for I_{dc} above. For N = 0 a J_o-like dependence of the dc supercurrent with microwave power has been observed and in addition it has been found that a singularity does occur as Werthamer stated at $f = E_g$.

11.3 Program for the Next Period. The next phase of this investigation will concentrate on making superconducting junctions both of the thin film and point-contact variety. It is hoped that a variety of materials applicable in the millimeter and submillimeter region can be used, and a circuit to measure the detection properties of such junctions can be developed. Calculations will also be performed on the mixing and self-mixing properties of these devices.